

# Oscillations of vertically integrated relativistic tori – II. Axisymmetric modes in a Kerr spacetime

Pedro J. Montero<sup>(1)</sup>, Luciano Rezzolla<sup>(1,2)</sup>, Shin'ichirou Yoshida<sup>(3,1)</sup>

<sup>(1)</sup>SISSA, International School for Advanced Studies and INFN, Via Beirut, 2 34014 Trieste, Italy

<sup>(2)</sup>Department of Physics and Astronomy, Louisiana State University, Baton Rouge, LA 70803 USA

<sup>(3)</sup>Department of Physics, University of Wisconsin-Milwaukee, Milwaukee, WI 53211, USA

7 November 2018

## ABSTRACT

This is the second of a series of papers investigating the oscillation properties of relativistic, non-selfgravitating tori orbiting around black holes. Extending the work done in a Schwarzschild background, we here consider the axisymmetric oscillations of vertically integrated tori in a Kerr spacetime. The tori are modeled with a number of different non-Keplerian distributions of specific angular momentum and we discuss how the oscillation properties depend on these and on the rotation of the central black hole. We first consider a local analysis to highlight the relations between acoustic and epicyclic oscillations in a Kerr spacetime and subsequently perform a global eigenmode analysis to compute the axisymmetric  $p$  modes. In analogy with what found in a Schwarzschild background, these modes behave as sound waves that are modified by rotation and are globally trapped in the torus. For constant distributions of specific angular momentum, the eigenfrequencies appear in a sequence 2:3:4:... which is essentially independent of the size of the disc and of the black hole rotation. For non-constant distributions of angular momentum, on the other hand, the sequence depends on the properties of the disc and on the spin of the black hole, becoming harmonic for sufficiently large tori. We also comment on how  $p$  modes could explain the high frequency quasi-periodic oscillations observed in low-mass X-ray binaries with a black hole candidate and the properties of an equivalent model in Newtonian physics.

**Key words:** accretion, accretion discs – black hole physics – hydrodynamics – relativity

## 1 INTRODUCTION

A recent series of papers (Font & Daigne, 2002a,b; Daigne & Font, 2004) has shown, through general relativistic hydrodynamic simulations, that the relativistic geometrically thick discs of high-density matter expected to form after the coalescence of a binary system of neutron stars or after the gravitational collapse of a rotating supermassive star may be subject to the runaway instability which could destroy the disc on a dynamical timescale (Abramowicz, Calvani and Nobili, 1983). Accretion tori of much smaller rest-mass densities have also been observed in three-dimensional general relativistic magnetohydrodynamic simulations investigating the properties of accretion flows onto Kerr black holes (De Villiers et al. 2003).

With the aim of assessing whether the onset of the runaway instability depends sensitively on the choice of initial conditions, Zanotti et al. (2003) carried out general relativistic hydrodynamic simulations of *perturbed* tori orbiting around a Schwarzschild black hole and shown that the instability may take place independently of the way the mass accretion is induced. In addition, the simulations have indicated how the introduction of perturbations triggers harmonic oscillations in the tori which could produce large

variations of their mass quadrupole. In the case in which the torus is made of high-density matter (as in the case of binary neutron star merger), these oscillations could then lead to the emission of gravitational waves with amplitudes comparable with those produced in a gravitational stellar-core collapse, thus making these objects promising sources of gravitational radiation even if the instability does not set in.

Together with the general relativistic hydrodynamic simulations, oscillation modes of geometrically thick relativistic discs can also be studied through perturbative analyses. Clearly, this second approach is computationally less intensive and allows therefore for a more detailed investigation of the parameter space. Using a linear perturbative approach, Rezzolla et al. (2003b; Paper I hereafter), have recently investigated the axisymmetric oscillation properties of relativistic tori in a Schwarzschild spacetime. To simplify the treatment and make it as analytical as possible, the tori were built with vertically integrated and vertically averaged quantities, thus transforming the eigenvalue problem into a set of coupled ordinary differential equations. The tori were then modeled with a number of different non-Keplerian distributions of specific angular momentum. Overall, the perturbative analysis of Paper I confirmed the re-

arXiv:astro-ph/0407642v1 30 Jul 2004

sults obtained by Zanotti et al. (2003) through nonlinear simulations, revealing that the oscillations found in the simulations correspond to  $p$  modes and that the lowest-order eigenfrequencies must be in a sequence of small integers 2:3:4..., rather independently of the size and the specific angular momentum distribution of the tori. Furthermore, a detailed study of the eigenfunctions in Paper I has also provided a possible explanation for the numerical evidence that the runaway instability can be efficiently suppressed for tori with distributions of specific angular momentum that follow a power-law (Font & Daigne, 2002b).

This paper intends to extend the work of Paper I and is therefore devoted to both a local and a global perturbative analysis of axisymmetric modes of oscillation of relativistic tori in the background spacetime of a Kerr black hole. While the local analysis provides us with the dispersion relation for inertial-acoustic waves in relativistic non-Keplerian discs, the global approach provides us with the eigenfunctions and eigenfrequencies of the  $p$ -mode oscillations of the system. As in Paper I, we have here removed one spatial dimension from the problem by considering vertically integrated tori and have neglected the variations in the background spacetime produced by the perturbations (*i.e.* Cowling approximation). Also in this case, therefore, the solution of the eigenvalue problem is simplified considerably and reduces to the solution of a single second-order ordinary differential equation.

Overall, the results found indicate that the  $p$ -mode oscillations of vertically integrated tori in a Kerr spacetime share many of the features already encountered in a Schwarzschild spacetime. In particular: the dependence of the fundamental eigenfrequencies on the position of the rest-mass density maximum and on the radial size of the discs, the relation of  $p$  modes with the radial epicyclic oscillations of point-like particles, or the simple 2:3 harmonic sequence for the lowest-order eigenfrequencies. Furthermore, this work extends to geometrically thick discs all of the relativistic disco-seismology analyses carried so far for thin discs (Okazaki et al., 1987; Perez et al., 1997; Silbergleit et al., 2001; Kato, 2001, Rodriguez et al., 2002).

The oscillations of geometrically thick discs are important not only because they could produce intense gravitational radiation, but also because, in low-density discs, they may serve to explain the high-frequency quasi-periodic oscillations (HFQPOs) observed in low-mass X-ray binaries (LMXBs) containing a black hole candidate. In these systems, in fact, the X-ray luminosity is modulated quasi-periodically, giving rise to distinctive peaks in the power spectral density which, so far, have been found in sequences of small integers 2:3 (see Abramowicz and Kluźniak, 2001 for the interpretation of the results of Remillard et al., 1999 and Strohmayer, 2001; see Remillard et al., 2002, Homan et al., 2003 for further observational evidences). More recently and although with a much poorer statistics, the possible presence of a QPO structure has been suggested also in the power spectrum of the light curve of the two brightest X-ray flares from the Galactic Center black hole (Aschenbach et al., 2004).

Using the striking analogy between the results of the numerical simulations and the observations in LMXBs, Rezzolla et al. (2003a) have proposed a simple model that exploits the properties of  $p$ -mode oscillations in thick discs and accounts for the complex phenomenology observed for HFQPOs. It is interesting to note while such a configuration could be produced whenever an intervening process modifies the Keplerian character of the flow near the black hole, the numerical simulations of De Villiers et al. (2003) have now provided a more realistic clue to how these tori can be generated. Similarly, the recent model proposed by Gian-

nios & Spruit (2004) suggests a simple way in which these  $p$ -mode oscillations could be excited. Both of these models were not available at the time the model by Rezzolla et al. (2003a) was proposed.

To further develop this idea, we have here considered whether a purely Newtonian description of physics could be sufficient to account for the observations. For studying this, we have also performed a global analysis of the axisymmetric oscillations of vertically integrated non-Keplerian discs in Newtonian physics. Our results indicate that no major *qualitative* differences emerge and that the most important features of  $p$  modes in relativistic tori remain unchanged also in the corresponding Newtonian models, albeit with *quantitative* differences.

The plan of the paper is as follows: in Section 2 we introduce the basic assumptions and equations employed in the definition of our general relativistic, vertically integrated tori. These equations will then be used to study axisymmetric oscillations both locally, in Section 3, and globally, in Section 4. We will first consider configurations with constant distributions of specific angular momentum and subsequently distributions in the cylindrical radial coordinate distributions of specific angular momentum that increase outwards as power-laws. In Section 5 we comment on how these axisymmetric oscillations can be used to explain the HFQPOs in LMXBs containing a black hole and discuss the solution of the eigenvalue problem for vertically integrated Newtonian tori. Finally, Section 6 contains our conclusions.

Hereafter, Greek indices are taken to run from 0 to 3 and Latin indices from 1 to 3; unless stated differently, we will use units in which  $G = c = M_{\odot} = 1$ .

## 2 RELATIVISTIC TORI IN A KERR SPACETIME: ASSUMPTIONS AND EQUATIONS

We will here assume that the torus does not contribute to the spacetime metric, which we will take to be that external to a Kerr black hole. Furthermore, since we are interested in the portion of the spacetime in the vicinity of the equatorial plane (*i.e.* for values of the spherical angular coordinate  $|\theta - \pi/2| \ll 1$ ), we will write the Kerr metric in cylindrical coordinates  $(t, \varpi, \phi, \theta)$  and retain the zeroth-order terms in the ratio  $(z/\varpi)$ . In this case, the line element assumes the form (Novikov and Thorne 1973)

$$ds^2 = -\frac{\varpi^2 \Delta}{A} dt^2 + \frac{A}{\varpi^2} (d\phi - \omega dt)^2 + \frac{\varpi^2}{\Delta} d\varpi^2 + dz^2, \quad (1)$$

where  $A \equiv \varpi^4 + \varpi^2 a^2 + 2M\varpi a^2$ ,  $\Delta \equiv \varpi^2 - 2M\varpi + a^2$  and  $\omega \equiv 2Ma\varpi/A$ . Here,  $M$  is the gravitational mass of the black hole and  $a/M$  is the Kerr parameter, so that the black hole angular momentum can be expressed as  $J = aM$ .

The basic equations to be solved to construct models in hydrostatic equilibrium are the continuity equation  $\nabla_{\alpha}(\rho u^{\alpha}) = 0$  and the conservation of energy-momentum,  $\nabla_{\alpha} T^{\alpha\beta} = 0$ , where the symbol  $\nabla$  refers to a covariant derivative with respect to the metric (1). Here,  $T^{\alpha\beta} \equiv (e + p)u^{\alpha}u^{\beta} + pg^{\alpha\beta}$  are the components of the stress-energy tensor of a perfect fluid, with  $u^{\alpha}$  being the components of the 4-velocity,  $\rho$  the rest-mass density,  $e$  the energy density and  $p$  the pressure. It is also useful to introduce an orthonormal tetrad carried by the local stationary observer and defined by the one-forms with components

$$\begin{aligned} \omega^{\hat{t}} &= \varpi \sqrt{\Delta/A} dt, & \omega^{\hat{\phi}} &= \sqrt{A} (d\phi - \omega dt) / \varpi, \\ \omega^{\hat{z}} &= dz, & \omega^{\hat{\varpi}} &= \varpi / \sqrt{\Delta} d\varpi. \end{aligned} \quad (2)$$

In this frame, the components of the four velocity of the fluid are

denoted by  $u^{\hat{i}}$  and the 3-velocity components are defined as

$$v^{\hat{i}} \equiv \frac{u^{\hat{i}}}{u^{\hat{t}}} = \frac{\omega_{\alpha}^{\hat{i}} u^{\alpha}}{\omega_{\alpha}^{\hat{t}} u^{\alpha}}, \quad i = \varpi, z, \phi. \quad (3)$$

We consider the perfect fluid to follow a polytropic equation of state (EOS)  $p = k\rho^{\gamma}$ , where  $k$  and  $\gamma \equiv d \ln p / d \ln \rho$  are the polytropic constant and the adiabatic index, respectively. Next, being interested in a vertically-integrated description of the torus, we introduce a *vertically integrated* pressure

$$P(\varpi) \equiv \int_{-H}^H p dz, \quad (4)$$

and a vertically integrated rest-mass density

$$\Sigma(\varpi) \equiv \int_{-H}^H \rho dz, \quad (5)$$

where  $H = H(\varpi)$  is the local ‘‘thickness’’ of the torus. We further assume that  $P$  and  $\Sigma$  obey an ‘‘effective’’ polytropic EOS

$$P = \mathcal{K} \Sigma^{\Gamma}, \quad (6)$$

so that  $\mathcal{K}$  and  $\Gamma \equiv d \ln P / d \ln \Sigma$  play the role of the polytropic constant and of the adiabatic index, respectively. As mentioned in Paper I, it is important to underline that (6) does not represent a vertically integrated polytropic EOS since the polytropic exponent  $\Gamma = \Gamma(\varpi)$  is now a function of the position inside the torus.

After the vertical integration, we enforce the conditions of hydrostatic equilibrium and axisymmetry (*i.e.* assume  $\partial_t = 0 = \partial_{\phi}$ ) and simplify the equation of energy-momentum conservation to a Bernoulli-type form (Kozłowski et al., 1978)

$$\frac{\nabla_i p}{e + p} = -\nabla_i \ln(u_t) + \frac{\Omega \nabla_i \ell}{1 - \Omega \ell}, \quad (7)$$

where  $\ell \equiv -u_{\phi}/u_t$  is the specific angular momentum (*i.e.* the angular momentum per unit energy). Using the only relevant component of equations (7), we construct the equilibrium model for a non-selfgravitating torus in the Kerr spacetime through the force-balance equation

$$\frac{1}{E + P} \frac{dP}{d\varpi} = -\frac{M(1 - a\Omega)^2/\varpi^2 - \varpi\Omega^2}{\varpi^2 \Delta / A - A(\omega - \Omega)^2/\varpi^2}, \quad (8)$$

where  $E$  is the vertically integrated energy density (*cf.* eq. 4).

We next perturb the hydrodynamical equations introducing Eulerian perturbations of the hydrodynamical variables with a harmonic time dependence of the type

$$\left( \delta V^{\hat{\varpi}}, \delta V^{\hat{\phi}}, \delta Q \right) \sim \exp(-i\sigma t), \quad (9)$$

where  $\delta Q \equiv \delta P / (E + P)$  and where we have defined the vertically averaged velocity perturbations respectively as

$$\delta V^{\hat{\varpi}} \equiv \frac{1}{2H} \int_{-H}^H \delta v^{\hat{\varpi}} dz, \quad \delta V^{\hat{\phi}} \equiv \frac{1}{2H} \int_{-H}^H \delta v^{\hat{\phi}} dz. \quad (10)$$

As in our previous investigation in a Schwarzschild spacetime, we assume that the Eulerian perturbations in the metric functions can be neglected, *i.e.*  $\delta g_{ab} = 0$  (Cowling approximation; Cowling, 1941). While this condition does not hold true in general, it represents a very good approximation in the case of non-selfgravitating tori.

Introducing now the quantities

$$\delta U \equiv i\delta V^{\hat{\varpi}}, \quad \delta W \equiv \delta V^{\hat{\phi}}, \quad (11)$$

to eliminate the imaginary part from the system of equations and

after a bit of straightforward algebra, we derive the following set of ordinary differential equations

$$\begin{aligned} \sigma \frac{\Delta}{\sqrt{A}} \delta U + \alpha \frac{\Delta}{\varpi^2} \delta Q' + \left[ \frac{\Delta^{3/2}}{A} \left( \frac{A}{\varpi^2} \right)' \Omega - \right. \\ \left. \frac{\Delta^{3/2}}{A} \left( \frac{A\omega}{\varpi^2} \right)' + 2 \frac{\Delta^{3/2}}{\varpi^2} (\Omega - \omega) \frac{P'}{E + P} \right] \delta W = 0, \end{aligned} \quad (12)$$

$$\begin{aligned} \sigma \frac{\varpi^2 \sqrt{\Delta}}{A} \delta W + \left\{ \Omega' + \Omega \left[ \ln \left( \frac{A}{\varpi^2} \right)' + \frac{A^2 \omega \omega'}{\varpi^4 \Delta} \right] + \right. \\ \left. \frac{A}{\varpi^2 \Delta} \left[ \left( \frac{\varpi^2 \Delta}{A} \right)' - \left( \frac{A\omega^2}{\varpi^2} \right)' + \omega \left( \frac{A\omega}{\varpi^2} \right)' \right] (\omega - \Omega) - \right. \\ \left. \frac{A^2 \omega'}{\varpi^4 \Delta} \Omega^2 - \frac{\varpi^2}{A} \left( \frac{A\omega}{\varpi^2} \right)' \right\} \frac{\Delta}{\sqrt{A}} \delta U + \frac{A\sigma\alpha}{\Delta\varpi^2} (\omega - \Omega) \delta Q = 0, \end{aligned} \quad (13)$$

$$\begin{aligned} \sigma \delta Q + \tilde{\Gamma} \frac{\Delta}{\sqrt{A}} \delta U' + \left\{ \frac{\Delta}{\sqrt{A}} \left[ \frac{P'}{E + P} + \right. \right. \\ \left. \left. \tilde{\Gamma} \left( \frac{1}{\varpi} - \frac{1}{2} \ln \left( \frac{r^2 \Delta}{A} - \frac{A}{\varpi^2} (\omega - \Omega)^2 \right) \right)' \right] + \right. \\ \left. \tilde{\Gamma} \left( \frac{\Delta}{\sqrt{A}} \right)' \right\} \delta U - \left( \frac{\sigma \sqrt{\Delta} (\omega - \Omega) A \varpi^2}{\varpi^4 \Delta - A^2 (\omega - \Omega)^2} \right) \tilde{\Gamma} \delta W = 0, \end{aligned} \quad (14)$$

where  $\alpha \equiv 1/(u^t)^2$ ,  $\tilde{\Gamma} \equiv \Gamma P / E + P$ , and the index  $'$  indicates a radial derivative.

Equations (12)–(14) are the  $\varpi$ - and  $\phi$ -components of the perturbed relativistic Euler equations and the perturbed continuity equation, respectively. As in Paper I, they are solved numerically for the eigenfrequencies and eigenfunctions of  $p$ -mode oscillations of an oscillating vertically integrated thick disc in a Kerr spacetime. Before discussing the solution of this eigenvalue problem, however, it is instructive to consider how wave-like perturbations propagate in the torus.

### 3 PERTURBATIONS OF RELATIVISTIC TORI: A LOCAL ANALYSIS

We now present a local analysis of the perturbed hydrodynamical equations (12)–(14) which will serve to clarify the relation between acoustic waves and other waves that play a fundamental role in fluids orbiting in a central potential, *i.e.* inertial (or epicyclic) waves. For this analysis we assume a harmonic radial dependence in the perturbed fluid quantities of the type  $(\delta Q, \delta U, \delta W) \sim \exp(ik\varpi)$ , where  $k$  is the radial wavenumber so that the local wavelength is  $\lambda = 2\pi/k$ .

To make the system of equations simpler, we have removed from equations (12)–(14) those terms that are much smaller than the others. Details on these simplifications are discussed in the Appendix A. The linearized perturbation equations (12)–(14) resulting from this procedure can thus be written as a homogeneous linear system in matrix form

$$\mathbf{M}(k, \sigma) \begin{pmatrix} \delta U \\ \delta W \\ \delta Q \end{pmatrix} = 0, \quad (15)$$

where  $\mathbf{M}$  is the coefficient matrix given by

$$\mathbf{M}(k, \sigma) = \begin{pmatrix} \frac{\sigma \Delta}{\sqrt{A}} & \frac{\Delta^{\frac{3}{2}}}{A} \left[ \Omega \left( \frac{A}{r^2} \right)' - \left( \frac{A\omega}{r^2} \right)' + \frac{2A(\Omega - \omega)P'}{r^2(E+P)} \right] & \frac{ik\alpha\Delta}{r^2} \\ \frac{H\Delta}{\sqrt{A}} & \frac{\sigma r^2 \sqrt{\Delta}}{A} & 0 \\ \frac{ik\tilde{\Gamma}\Delta}{\sqrt{A}} & 0 & \sigma \end{pmatrix} \quad (16)$$

The dispersion relation is then obtained by imposing the determinant of  $\mathbf{M}$  to be zero, thus guaranteeing that a non-trivial solution to the system of equations (15) exists. After a bit of algebra one obtains the dispersion relation

$$\sigma^2 = \kappa_r^2 + \frac{\Delta}{\varpi^2} \left[ \frac{\varpi^2 \Delta}{A} - \frac{A(\omega^2 + \Omega^2)}{\varpi^2} \right] k^2 c_s^2, \quad (17)$$

where  $c_s \equiv \sqrt{dP/dE}$  is the relativistic sound speed within the vertically integrated disc and where the relativistic radial epicyclic frequency for an extended fluid object in a Kerr spacetime  $\kappa_r$  is defined as

$$\kappa_r^2 \equiv \frac{\Delta C}{\varpi^2} \left[ \left( \frac{A}{\varpi^2} \right)' \Omega - \left( \frac{A\omega}{\varpi^2} \right)' + \frac{2A}{\varpi^2} (\Omega - \omega) \frac{P'}{E+P} \right]. \quad (18)$$

Here, the quantity  $C$  is just a shorthand for

$$C \equiv \frac{A(\omega - \Omega)}{\varpi^2 \Delta} \left[ \left( \frac{\varpi^2 \Delta}{A} \right)' - \left( \frac{A\omega^2}{\varpi^2} \right)' + \omega \left( \frac{A\omega}{\varpi^2} \right)' \right] + \Omega \left[ \ln \left( \frac{A}{\varpi^2} \right)' + \frac{A^2 \omega \omega'}{\Delta \varpi^4} - \frac{\Omega A^2 \omega'}{\Delta \varpi^4} \right] + \Omega' - \frac{\varpi^2}{A} \left( \frac{A\omega}{\varpi^2} \right)' \quad (19)$$

Equations (17) and (18) include corrections coming from the rotation of the black hole and pressure gradients from the fluid distribution and reduce respectively to the dispersion relation and to the relativistic epicyclic frequency for an extended object obtained in Paper I for a Schwarzschild black hole (*cf.* eqs. 42 and 43 of Paper I). When the motion is almost Keplerian, the pressure gradients are negligible and expression (18) reduces to the expression for the radial epicyclic frequency for point-like particles (Okazaki et al., 1987)

$$(\kappa_r^2)_{\text{Kep}} = \frac{M}{\varpi^3} \left[ \frac{1 - 6M/\varpi \pm 8a\sqrt{M/\varpi^3} - 3a^2/\varpi^2}{(1 \pm 8a\sqrt{M/\varpi^3})^2} \right], \quad (20)$$

where the  $\pm$  sign distinguishes orbits that are corotating from those that counter-rotating relative to the black hole spin.

The behaviour of the radial epicyclic frequency (20) is shown in Fig. 1 where different curves refer to different black hole spins and where we consider corotating orbits only. For each curve, furthermore, a dashed line refers to the “increasing” branch (*i.e.* with  $\kappa_r' > 0$ ), while a solid line refers to the “decreasing” branch (*i.e.* with  $\kappa_r' < 0$ ). The solid circles indicate the locations of the maximum frequencies for each black hole spin and will be used subsequently in Fig. 3. Finally, the dotted line indicates the Newtonian radial epicyclic frequency which will be used for the discussion in Section 5.1. The numerical values refer

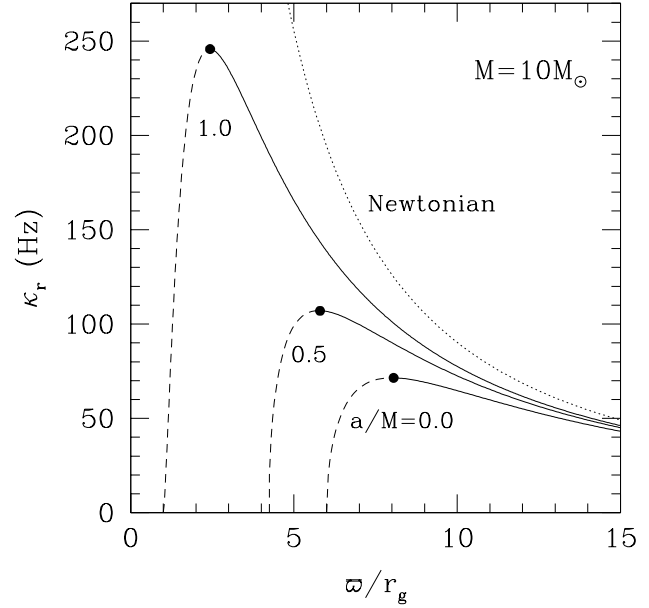


**Figure 1.** Radial epicyclic frequency for different values of the black hole spin. In each curve, a dashed line refers to the “increasing” branch (*i.e.* with  $\kappa_r' > 0$ ), while a solid line to the “decreasing” branch (*i.e.* with  $\kappa_r' < 0$ ). Indicated with solid circles are the locations of the maximum frequencies for each black hole spin, while the dotted line refers to the Newtonian values for the radial epicyclic frequency. The numerical values have been computed for a black hole with mass  $M = 10M_\odot$  and the radial extents have been expressed in units of gravitational radii  $r_g \equiv GM/c^2$ .

to a black hole with mass  $M = 10M_\odot$  and the radial extents have been expressed in units of gravitational radii  $r_g \equiv GM/c^2$ .

Overall, the dispersion relation (17) shows that the propagation of small perturbations in a fluid rotating around a Kerr black hole is characterized by two main features. The first one is of purely acoustic nature (*i.e.* with  $\sigma \propto kc_s$ ); the second one is of purely inertial nature (*i.e.* with  $\sigma \propto \kappa_r$ ) and is reminiscent of the oscillations that a particle orbiting in a central potential experiences when perturbed. For these reasons, the resulting waves are usually referred to as *inertial-acoustic waves* and the corresponding modes can be classified as *p* modes. The determination of the eigenfrequencies and eigenfunctions of these modes will be discussed in the following Section.

#### 4 PERTURBATIONS OF RELATIVISTIC TORI: A GLOBAL ANALYSIS

We now turn to a global analysis of the axisymmetric oscillation of relativistic tori in a Kerr spacetime by solving the system of equations (12)–(14) as an eigenvalue problem. In particular, the solution is found using a “shooting” method (Press et al., 1986) in which, once the appropriate boundary conditions are provided, two trial solutions are found, starting from inner and outer edges of the disc respectively, and these are then matched at an intermediate point where the Wronskian of the two solutions is evaluated (see Paper I for details). This procedure is iterated until a zero of the Wronskian is found, thus providing a value for  $\sigma$  and a solution for  $\delta Q$ ,  $\delta U$ , and  $\delta W$ . The numerical methods employed here to solve the eigen-

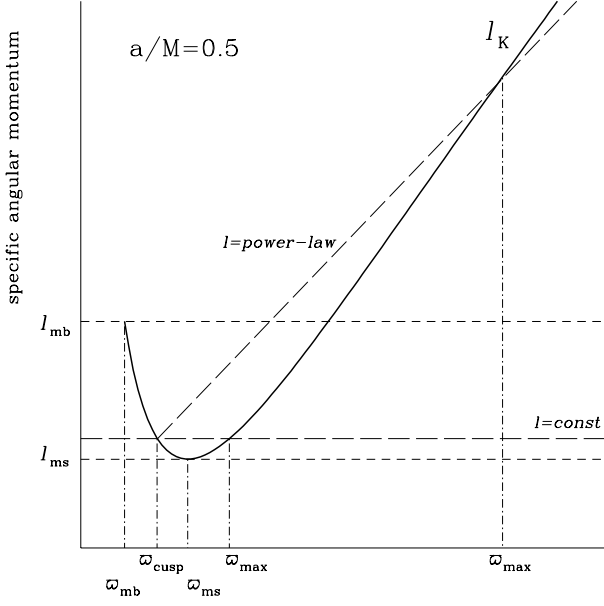


**Figure 2.** Schematic representation of the position of the relevant radii in the cases of “constant” and “power-law” distributions of specific angular momentum. In particular, while  $\varpi_{\text{cusp}}$  and  $\varpi_{\text{max}}$  indicate the positions of the cusp and of the rest-mass density maximum,  $\varpi_{\text{mb}}$  and  $\varpi_{\text{ms}}$  indicate the positions of the marginally bound and marginally stable orbits.

value problem are the same as those discussed in Paper I, where a more detailed discussion can be found.

It is useful to briefly summarize how the background model for the torus is constructed (see also Paper I) as this will help clarifying the discussion of the results presented in the following Sections. First of all, a value of the black hole spin  $a/M$  is chosen and the distribution of the specific angular momentum  $\ell = \ell(\varpi)$  is selected. The positions of the cusp and of the maximum rest-mass density in the torus are then obtained by imposing that the specific angular momentum at these two points coincides with the Keplerian value (see Fig. 2 for a schematic view). The inner edge of the torus  $\varpi_{\text{in}}$  is determined by fixing the potential gap,  $\Delta W_{\text{in}} = W_{\text{in}} - W_{\text{cusp}}$ , defined as

$$\Delta W_{\text{in}} = \ln[(-u_t)_{\text{in}}] - \ln[(-u_t)_{\text{cusp}}] - \int_{\ell_{\text{cusp}}}^{\ell_{\text{in}}} \frac{\Omega d\ell}{1 - \Omega\ell}, \quad (21)$$

with  $\Delta W_{\text{in}} = 0$  corresponding to a torus filling its outermost equipotential surface. Next, the hydrostatic balance equation (8) is integrated from  $\varpi_{\text{in}}$  to the outer edge of the torus  $\varpi_{\text{out}}$ , defined as the position at which  $P = 0$ . Sequences of tori having different radial extents for a given distribution of specific angular momentum and black hole spin can then be constructed by varying the potential gap  $\Delta W_{\text{in}}$ . In such sequences, the tori will have the same rest-density maxima  $\varpi_{\text{max}}$ .

Clearly, different distributions of specific angular momentum will produce tori with different positions of the cusp and of the maximum rest-mass density. In order to investigate how the axisymmetric oscillations depend on these properties, we have constructed models with different distributions of specific angular momentum, taken to be either constant within the torus, or increasing outwards according to a generic power-law in radius (*cf.* eq. 24). The main properties of the various models considered are summarized in Table 1, where they are presented in terms of dimension-

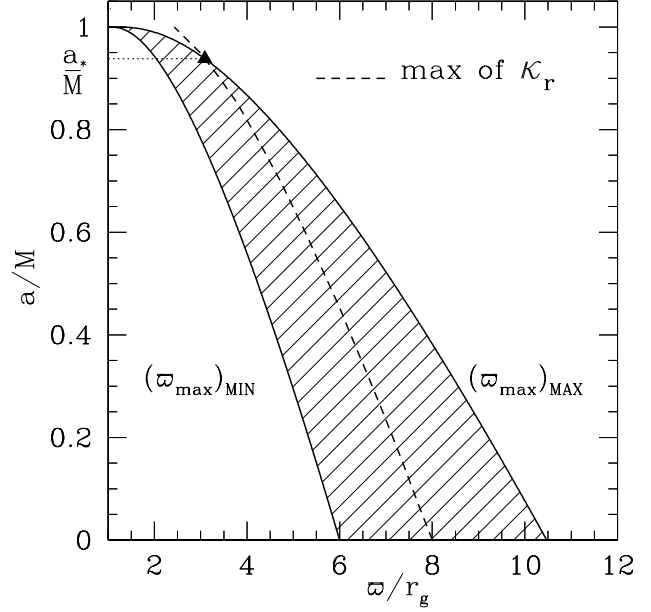


**Figure 3.** Possible locations of the rest-mass density maximum  $\varpi_{\text{max}}$  for tori with constant specific angular momentum distribution and for all possible black hole spins. The solid lines refer to the smallest and largest possible positions of  $\varpi_{\text{max}}$ , while the dashed line indicates the locations of the maximum of epicyclic frequency  $\kappa_r$  (*cf.* the solid circles in Fig. 1).

less quantities. A simple conversion of the dimensionless eigenfrequency  $\tilde{\sigma}$  and of the specific angular momentum  $\tilde{\ell}$  is obtained, for instance, through the following relations

$$\sigma = \tilde{\sigma} \left( \frac{M}{M_{\odot}} \right)^{-1} \left( \frac{GM_{\odot}}{c^2} \right)^{-1} c, \quad (22)$$

and

$$\ell = \tilde{\ell} \left( \frac{M}{M_{\odot}} \right) \left( \frac{GM_{\odot}}{c^2} \right) c. \quad (23)$$

## 4.1 Constant specific angular momentum tori

### 4.1.1 Fixed black hole spin

We first consider tori with a distribution of specific angular momentum that is constant in space, *i.e.*  $\ell(\varpi) = \text{const.}$ , not only because this choice is mathematically simpler to investigate, but also because it allows for a straightforward determination of the permitted range of equilibrium models. In this case, in fact, for a torus of finite size to exist, the value of the specific angular momentum must satisfy  $\ell_{\text{ms}} < \ell < \ell_{\text{mb}}$ , where  $\ell_{\text{ms}}$  and  $\ell_{\text{mb}}$  are the specific angular momenta of the marginally stable and of the marginally bound orbit, respectively. For a Schwarzschild black hole,  $\ell_{\text{ms}} = 3\sqrt{6}/2 \sim 3.67$  and  $\ell_{\text{mb}} = 4$ , while they depend of the the black hole spin for a Kerr black hole. Because the position of the rest-mass density maximum  $\varpi_{\text{max}}$  will depend on the specific value of  $\ell$  chosen, it is then possible to define the range in which  $\varpi_{\text{max}}$  lies. In other words, all of the possible finite-size tori will have  $(\varpi_{\text{max}})_{\text{MIN}} < \varpi_{\text{max}} < (\varpi_{\text{max}})_{\text{MAX}}$ , where we have defined  $(\varpi_{\text{max}})_{\text{MIN}}$  as the value of  $\varpi_{\text{max}}$  when  $\ell = \ell_{\text{ms}}$ , and  $(\varpi_{\text{max}})_{\text{MAX}}$  as the value of  $\varpi_{\text{max}}$  when  $\ell = \ell_{\text{mb}}$ . Clearly,  $(\varpi_{\text{max}})_{\text{MIN}}$  also coincides with the location of the marginally stable orbit, while

## 6 *Montero, Rezzolla and Yoshida*

**Table 1.** Main properties of the equilibrium models studied. From left to right the columns show: the black hole spin parameter, the type of specific angular momentum distribution, the constant coefficient  $\ell_c$  and the power-law index  $q$  (cf. eq. 24), the position of the maximum density point  $\tilde{\varpi}_{\max}$ , the position of the inner and outer radii of the torus  $\tilde{\varpi}_{\text{in}}$  and  $\tilde{\varpi}_{\text{out}}$ , the position of the maximum density point with respect to the epicyclic frequency curve, and the potential gap at the inner edge of the torus  $\Delta W_{\text{in}}$ . This latter quantity is reported because not all equilibrium models reported in this table have been constructed as the ones filling the largest closed equipotential surface (*i.e.* P16–P19).

Model	$a/M$	$\ell(\varpi)$ – distribution	$\tilde{\ell}_c$	$q$	$\tilde{\varpi}_{\max}$	$\tilde{\varpi}_{\text{in}}$	$\tilde{\varpi}_{\text{out}}$	$L$	$\kappa'_r$ at $\tilde{\varpi}_{\max}$	$\Delta W_{\text{in}}$
C1a	0.5	const.	3.283	0.0	6.01	3.21	13.26	10.04	$< 0$	$-1.0 \times 10^{-10}$
C1b	0.5	const.	3.313	0.0	6.29	3.13	18.04	14.92	$< 0$	$-1.0 \times 10^{-10}$
C1c	0.5	const.	3.343	0.0	6.55	3.05	26.66	23.60	$< 0$	$-1.0 \times 10^{-10}$
C1d	0.5	const.	3.373	0.0	6.81	2.99	47.78	44.79	$< 0$	$-1.0 \times 10^{-10}$
C1e	0.5	const.	3.403	0.0	7.07	2.93	181.6	178.7	$< 0$	$-1.0 \times 10^{-10}$
C2a	0.5	const.	3.193	0.0	5.00	3.65	6.330	2.680	$> 0$	$-1.0 \times 10^{-10}$
C2b	0.5	const.	3.207	0.0	5.20	3.54	7.128	3.583	$> 0$	$-1.0 \times 10^{-10}$
C2c	0.5	const.	3.223	0.0	5.39	3.45	8.079	4.627	$> 0$	$-1.0 \times 10^{-10}$
C2d	0.5	const.	3.253	0.0	5.71	3.32	10.22	6.896	$> 0$	$-1.0 \times 10^{-10}$
C3a	0.0	const.	3.704	0.0	7.0	5.22	8.572	3.354	$< 0$	$-1.0 \times 10^{-10}$
C3b	0.1	const.	3.637	0.0	7.0	4.71	9.566	4.851	$< 0$	$-1.0 \times 10^{-10}$
C3c	0.2	const.	3.573	0.0	7.0	4.24	11.18	6.946	$< 0$	$-1.0 \times 10^{-10}$
C3d	0.3	const.	3.511	0.0	7.0	3.79	14.27	10.48	$< 0$	$-1.0 \times 10^{-10}$
C3e	0.4	const.	3.452	0.0	7.0	3.36	22.40	19.04	$< 0$	$-1.0 \times 10^{-10}$
C3f	0.5	const.	3.395	0.0	7.0	2.95	103.1	100.2	$< 0$	$-1.0 \times 10^{-10}$
C4a	0.5	const.	3.167	0.0	4.5	3.99	4.821	0.828	$< 0$	$-1.0 \times 10^{-10}$
C4b	0.6	const.	3.060	0.0	4.5	3.32	5.650	2.330	$< 0$	$-1.0 \times 10^{-10}$
C4c	0.7	const.	2.960	0.0	4.5	2.70	7.879	5.173	$< 0$	$-1.0 \times 10^{-10}$
C4d	0.8	const.	2.867	0.0	4.5	2.14	32.55	30.39	$< 0$	$-1.0 \times 10^{-10}$
P10	0.0	power-law	3.381	0.06	9.0	5.02	15.92	10.90	$< 0$	$-1.0 \times 10^{-10}$
P11	0.1	power-law	3.120	0.09	9.0	4.97	16.04	11.08	$< 0$	$-1.0 \times 10^{-10}$
P12	0.2	power-law	2.999	0.10	9.0	4.64	18.61	13.97	$< 0$	$-1.0 \times 10^{-10}$
P13	0.3	power-law	2.800	0.13	9.0	4.49	19.81	15.32	$< 0$	$-1.0 \times 10^{-10}$
P14	0.4	power-law	2.738	0.13	9.0	4.04	26.52	22.48	$< 0$	$-1.0 \times 10^{-10}$
P15	0.5	power-law	2.730	0.13	9.0	3.49	66.39	62.89	$< 0$	$-1.0 \times 10^{-10}$
P16	0.6	power-law	2.649	0.14	9.0	3.74	197.7	194.0	$< 0$	$-1.0 \times 10^{-2}$
P17	0.7	power-law	2.362	0.19	9.0	3.71	289.4	285.7	$< 0$	$-1.0 \times 10^{-2}$
P18	0.8	power-law	2.272	0.20	9.0	4.84	29.12	24.28	$< 0$	$-5.0 \times 10^{-2}$
P19	0.9	power-law	2.152	0.22	9.0	4.45	46.05	41.60	$< 0$	$-1.0 \times 10^{-1}$

$(\varpi_{\max})_{\text{MAX}}$  provides the position of the rest-mass density maximum for a torus whose outermost equipotential surface closes at infinity.

Furthermore, because in a Kerr spacetime the values of  $\ell_{\text{ms}}$  and  $\ell_{\text{mb}}$  will depend on the black hole spin  $a/M$ , it is possible to define the set of all the possible values that  $\varpi_{\max}$  can assume for constant angular momentum tori constructed in a Kerr spacetime. This is shown as a shaded area in Fig. 3, where we have also plotted with solid lines the different values of  $(\varpi_{\max})_{\text{MIN}}$  and  $(\varpi_{\max})_{\text{MAX}}$  as the black hole spin is increased from 0 to 1<sup>1</sup>. Also shown with a dashed line are the locations of the maximum of epicyclic frequency for different black hole spins (*cf.* the solid circles in Fig. 1).

Note that for tori with constant specific angular momentum distributions around rapidly rotating black holes with spin parameter  $a/M$  larger than  $a_*/M$  (*cf.* Fig. 3), all of the possible values of  $\varpi_{\max}$  will be located on the “increasing branch” of the epicyclic frequency (*i.e.* at positions where  $\kappa'_r > 0$ ). As a result, the closer the maximum density point is to the black hole horizon, the smaller the value of the epicyclic frequency at that point (*cf.* eq. 20). For rotations of the central black hole smaller than  $a_*/M$ , on the other

hand, the models with  $\varpi_{\max}$  in the “decreasing branch” of the epicyclic frequency (*i.e.* at positions where  $\kappa'_r < 0$ ) are also allowed together with those on the increasing branch. In this case, if the maximum rest-mass density point coincides with the location of the maximum point of the epicyclic frequency (*i.e.* at positions where  $\kappa'_r = 0$ ), the eigenfrequency of the fundamental mode for a given radial extent will have the largest value for any  $a < a_*$ . The locus of these points is indicated with a dashed line in Fig. 3.

In order to investigate the dependence of the fundamental mode of oscillation on the position of the maximum rest-mass density, we have first considered sequences of tori having different radial extents  $L \equiv \varpi_{\text{out}} - \varpi_{\text{in}}$ . All sequences are built for the same value of the black hole spin, while each sequence is characterized by a specific value of  $\varpi_{\max}$ , which is chosen to be either on the increasing or on the decreasing branch of the corresponding epicyclic frequency. The results for a black hole spin  $a/M = 0.5$  are summarized in the two panels of Fig. 4, which show the values of the eigenfrequency of the fundamental mode of oscillation  $f$  as a function of the disc radial extents  $L$ .

In the left panel, in particular, we show the results for models whose maximum rest-mass density is located on the decreasing branch of the radial epicyclic frequency. As expected for modes behaving effectively as sound waves trapped in a rotating fluid, the

<sup>1</sup> We have not considered here counterrotating black holes, *i.e.* with  $a < 0$ .

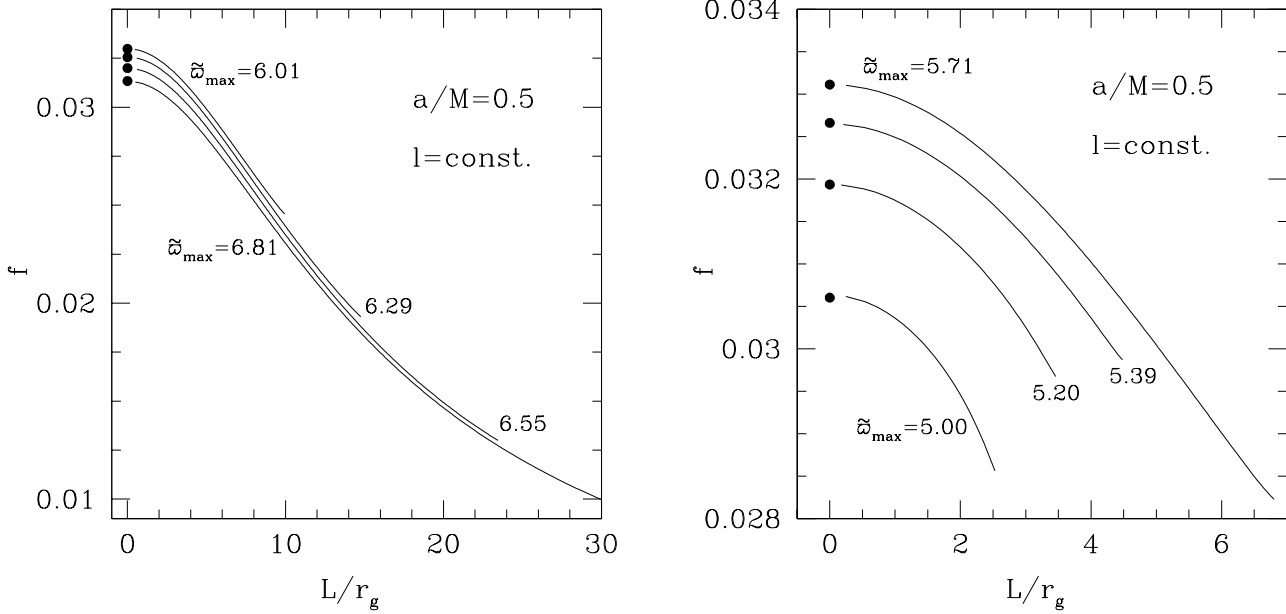


**Figure 4.** Eigenfrequencies for the fundamental mode of axisymmetric  $p$  modes for tori with a constant distribution of specific angular momentum. Each line corresponds to a sequence of tori having the same  $\varpi_{\max}$  but different radial extents  $L$  and the solid circles correspond to the values of the Keplerian radial epicyclic frequency (20) at  $\varpi_{\max}$ . Both panels refer to a Kerr black hole with  $a/M = 0.5$ , but while the right panel has  $\varpi_{\max}$  located in the increasing branch of the epicyclic frequency (*i.e.*  $\kappa_r' > 0$ ), the left one has  $\varpi_{\max}$  located in the decreasing branch of the epicyclic frequency (*i.e.*  $\kappa_r' < 0$ ).

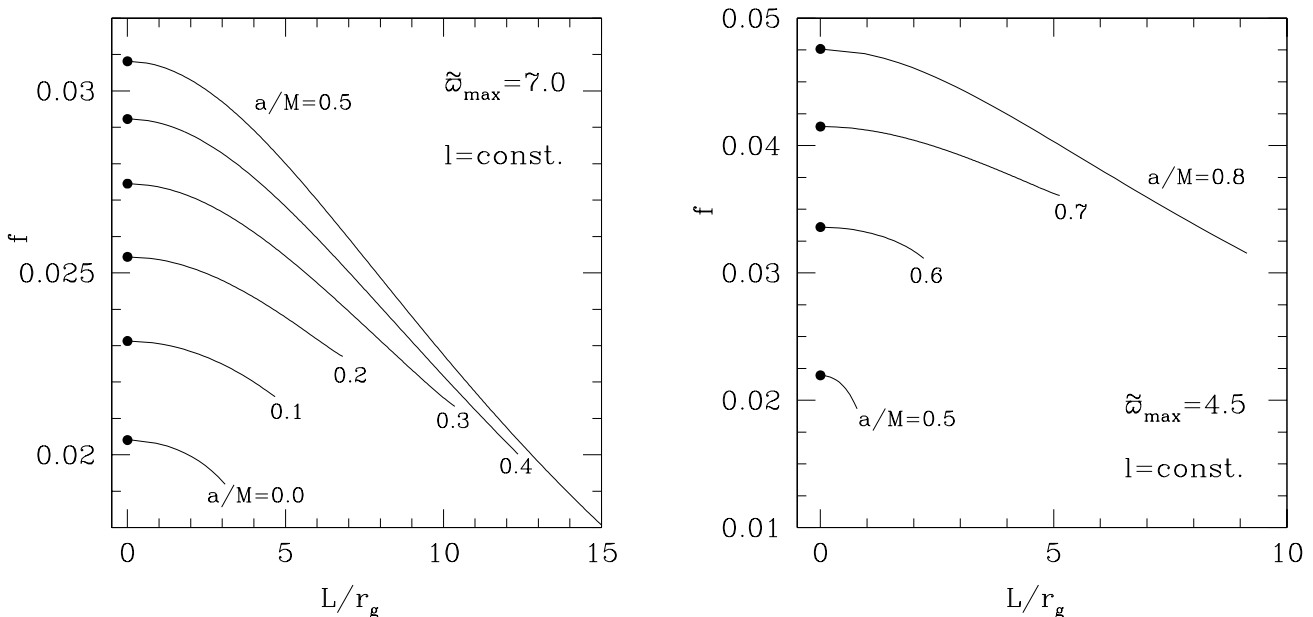


**Figure 5.** Eigenfrequencies for the fundamental mode of axisymmetric  $p$  modes for tori with a constant distribution of specific angular momentum. Each line refers to a sequence of tori for the same black hole spin  $a/M$ , but having different radial extents  $L$  and the solid circles correspond to the values of the Keplerian radial epicyclic frequency (20) at  $\varpi_{\max}$ . In each panel, the sequences have been computed keeping fixed the position of  $\varpi_{\max}$ , which are however different according to whether the black holes are slowly rotating (left panel) or rapidly rotating (right panel).

eigenfrequencies decrease like  $L^{-1}$  as the radial extent of the torus increases. Note also that, as was shown in Paper I for tori orbiting around a Schwarzschild black hole, the eigenfrequencies of the fundamental mode tend to the values of the radial epicyclic frequency at  $\varpi_{\max}$  as the radial dimension of the discs tends to zero

(In Figs. 4, 5 and 9 the filled circles show the values of the Keplerian radial epicyclic frequency (20) at  $\varpi_{\max}$ ). These results confirm the expectation that, as their size diminishes, the discs effectively behave as rings of particles in circular orbits and have as their char-

acteristic frequency the epicyclic frequency at the maximum rest-mass density point.

Note also in the left panel of Fig. 4 that models with the same radial extent and different constant angular momentum distributions, *i.e.*, tori with different locations of  $\varpi_{\max}$ , have fundamental eigenfrequencies that become larger as the rest-mass density maximum approaches the black hole. This behaviour can be explained simply since, for  $L \rightarrow 0$ , the fundamental eigenfrequencies converge to the values of the epicyclic frequencies and the latter increase for smaller radii as one moves along the decreasing branch.

The opposite behavior is observed in the right panel of Fig. 4, but in this case the maximum density point of all models is located on the increasing branch of the epicyclic frequency. As a result, models with the same radial extent have fundamental frequencies that become smaller as the rest-mass density maximum approaches the black hole. Therefore, for any given radial extent, the model with the largest fundamental-mode eigenfrequency will be the one with  $\varpi_{\max}$  located at the maximum of the epicyclic frequency (*i.e.* along the dashed line in Fig. 3).

#### 4.1.2 Influence of the black hole spin

In order to investigate the influence of the spin of the central black hole on the axisymmetric oscillations, we have solved the eigenvalue problem for sequences of tori having the same location of  $\varpi_{\max}$  but different black hole rotation rates.

We note that, in the case of constant specific angular momentum, it is not possible to construct sequences of tori having the same location of the rest-mass density maximum for all the possible values of the black hole spin. This is due to the fact that for any given  $\varpi_{\max}$ , the existence of marginally stable and marginally bound orbit limits the range of values that  $a/M$  can assume. This is quite apparent in Fig. 3 where, for any chosen value of  $\varpi_{\max}$ , the black hole spin cannot span the whole range from 0 to 1.

Because of this constraint, we show in the left panel of Fig. 5 sequences of tori having the same value of  $\varpi_{\max}/M = 7.0$  and black hole spins varying from  $a/M = 0.0$  to  $a/M = 0.5$ . Clearly, these sequences share many of the properties discussed for Fig. 4 and, in addition, for any given radial size of the torus, the frequency of the fundamental mode will be larger for larger black hole spin. Indeed, this is what is expected, since the radial epicyclic frequency for a point-like particle  $(\kappa_r)_{\text{Kep}}$  increases monotonically with  $a$  for any value of  $\varpi$  (*cf.* Fig. 1). The same behaviour is observed also when  $\varpi_{\max}/M = 4.5$ , which allows for larger rotation rates of the black hole and is shown in the right panel of Fig. 5.

#### 4.1.3 Harmonic Sequence

An interesting and potentially important feature of axisymmetric  $p$ -mode oscillations of tori with constant specific angular momentum is that the lowest-order eigenfrequencies appear in a sequence 2:3:4..., with a good accuracy (*i.e.* within 10%) and rather independently of the details of the disc properties. This feature was first discovered through the fully nonlinear numerical simulations of Zantoni et al. (2003) and subsequently confirmed through a perturbative analysis in a Schwarzschild spacetime in Paper I, and through additional independent numerical simulations (Kluźniak et al., 2004; Lee et al., 2004).

A harmonic relation for the lowest-order eigenfrequencies continues to exist also for tori with constant specific angular momentum in a Kerr spacetime and rather insensitively of the black

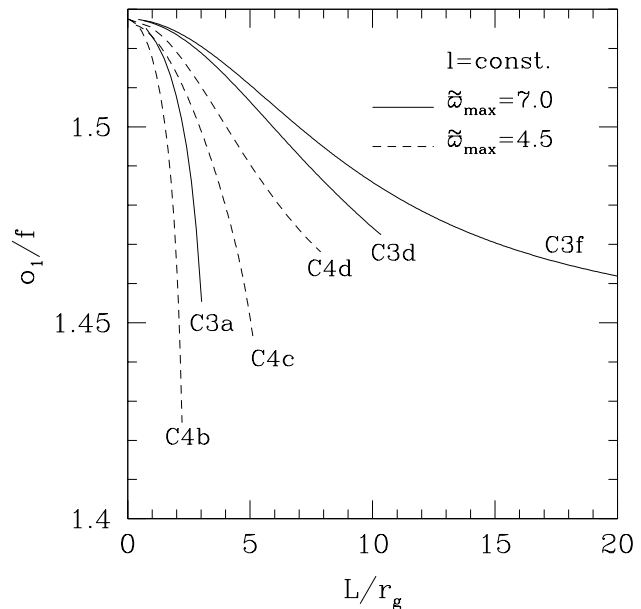


**Figure 6.** Ratio of the first overtone and the fundamental mode of oscillation for tori with constant specific angular momentum distributions. The different sequences refer to the different models described in Table 1, with the solid lines referring to  $\varpi_{\max} = 7.0 r_g$  and the dashed ones to  $\varpi_{\max} = 4.5 r_g$ .

hole spin. Fig. 6 shows the ratio between the frequencies of the first overtone  $o_1$  and the fundamental mode  $f$  for some representative tori with constant specific angular momentum distributions considered in Table 1. Different line types correspond to sequences that have been constructed with different locations of the rest-mass density maximum. All of the sequences span values of  $a/M$  from 0 to 0.8 without showing major qualitative differences.

Since it is not the result of a mathematical constraint but, rather, the consequence of a global mode of oscillation, the 2:3 ratio between the fundamental mode and its first overtone is satisfied with an accuracy that is in general within 10%, but is, nevertheless, not exact. A number of different elements can contribute to a deviation from an exact relation among integers and the results of our calculations show that conditions such as the size of the disc, the location of the rest-mass density maximum, the black hole spin, the distribution of specific angular momentum, or the EOS considered, can all influence this departure. Note also that in Fig. 6 some of the models (*e.g.* C4b and C3a) appear to have a rather large variation in the ratio  $o_1/f$ . It should be recalled, however, that these tori exist only over a very small range in the radial extent  $L$  (either because of the high value of the specific angular momentum or because of the large spin of the black hole). Being trapped in such small tori rather close to the black hole horizon where the angular velocity is larger, the  $p$ -mode oscillations will be particularly sensitive on variations of the radial size.

Another interesting feature of the lowest-order eigenfrequencies is that, for any given black hole rotation speed, their ratio tends to a single value  $o_1/f \sim 1.52$  as the size of the tori tends to zero (*cf.* Fig. 6). This is in good qualitative agreement with what was found in the perturbative analysis of slender tori (Blaes 1985), where the dispersion relation for generic perturbations of Newtonian slender tori having constant distributions of specific angular momentum, was derived (*cf.* eq. 1.8 of Blaes 1985, with  $j = 1$ , and  $|k| = 0$ ).



## 4.2 Non-constant specific angular momentum tori

We next investigate axisymmetric  $p$ -modes in tori with non-constant distributions of specific angular momentum. Clearly, in this case the problem is highly degenerate since there is a complete arbitrariness on what is the most appropriate distribution of angular momentum. The first guide in the infinite possible choices is that they should correspond to stable fluid configurations. While in Newtonian theory one can make use of the simple Rayleigh stability criterion for rotating inviscid fluids  $d\ell/d\varpi > 0$  (Tassoul 1978), the situation in a general relativistic framework is more complex. In particular, the condition of stability requires that, for the perfect fluids considered here, the gradient of the specific angular momentum must never point toward the interior of the quasi-circular level surfaces of  $\ell$  (Seguin 1975, Abramowicz and Prasanna 1985). Because of this, we have used a simple prescription for the specific angular momentum in which it increases outwards with a power-law distribution of the type

$$\tilde{\ell} = \ell_c \varpi^q, \quad (24)$$

where both  $\ell_c$  and  $q$  are positive constants (*cf.* Table 1 for the different values used).

Following the procedure presented in the previous Section, we have constructed tori by selecting the angular momentum distribution such that the position of the cusp is always located between the marginally bound and the marginally stable orbits. Note that, in principle, this is not the only possible choice. Non-constant distributions of specific angular momentum, in fact, allow for the construction of tori having the cusp at radii larger than the position of the marginally stable orbit. In such tori, matter lost through the cusp as a result of small perturbations would be able to find new stable circular orbits and, as a result, the accretion onto the black hole will require mechanisms other than simple perturbations in the flow. Here, we have not investigated the properties of these discs whose dynamics, however, has been considered in detail by Zanotti et al., (2004).

Overall, the solutions for tori with non-constant distributions of specific angular momentum share qualitative similarities with those found when  $\ell = \text{const}$ . In particular, the main properties of the  $p$ -mode oscillations in this case can be summarized as follows: Firstly, the eigenfrequencies depend on the location of the rest-mass density maximum  $\varpi_{\text{max}}$  and on whether the latter is located on the increasing or decreasing branch of the radial epicyclic frequency. Secondly, all eigenfrequencies tend to the radial epicyclic frequency at the location of  $\varpi_{\text{max}}$  in the limit of small tori. Thirdly, as the result of the presence of an *evanescent-wave* region (see Paper I for a detailed discussion), the eigenfunctions become vanishingly small at the inner edge of the disc, while they do not do so at the outer edge. Finally, for any sequence built with fixed  $\varpi_{\text{max}}$ , the eigenfrequencies increase as the spin of the black hole is increased.

Despite these similarities, a difference does emerge when investigating non-constant angular momentum tori. In this case, in fact, the ratio between the first overtone and the fundamental frequency of oscillation  $\omega_1/f$  has a behaviour which is more complex than the one found when  $\ell = \text{const}$ . In particular, it depends not only to the position of  $\varpi_{\text{max}}$ , but also on the values of  $\ell_c$  and  $q$ , as well as on  $a/M$ . Most importantly, while the eigenfrequencies remain in a harmonic sequence for sufficiently large discs, departures from a 2:3 ratio can be observed for very small discs. This is shown in Fig.7, where the  $\omega_1/f$  ratio is plotted for sequences of models orbiting around central black holes rotating at different rates and having different distributions of specific angular momentum (see

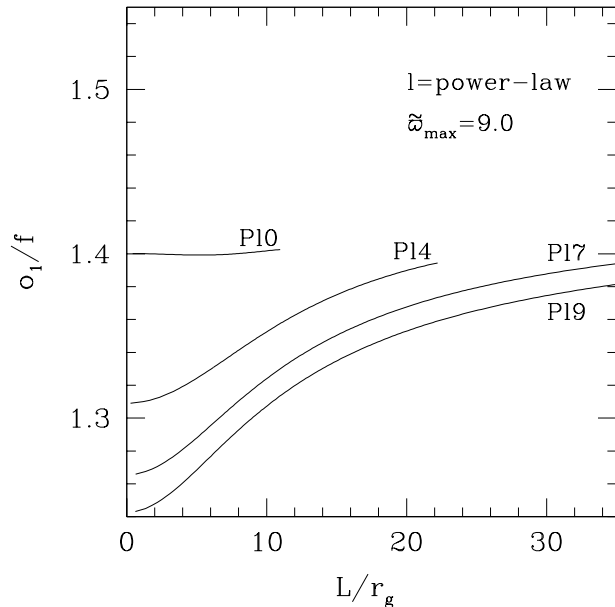


**Figure 7.** Ratio of the first overtone and the fundamental mode of oscillation for tori with a power-law distribution of specific angular momentum. The different sequences distinguish different choices of the index  $q$ , but all refer to the same value for  $\ell_c$  (*cf.* Table 1).

Table 1 for the model descriptions). In all the cases considered, however, the departure from a 2:3 ratio is less than 20%.

Finally, note that, as the size of the discs tends to zero, the ratios do not tend to the same value, as was the case for constant specific angular momentum tori but, rather, to a value that depends on the index  $q$  of the power-law. This is shown in Fig. 8, where we illustrate results for sequences of tori with the same  $\ell_c$  but different indices  $q$ , built around the same Kerr black hole with  $a/M = 0.5$ . Also in this case, a closer agreement with a harmonic relation between the lowest-order eigenfrequencies is recovered for sufficiently large discs.

## 5 IMPLICATIONS FOR HFQPOS IN LMXBS

Observations of X-ray emissions from binary systems comprising a stellar-mass compact object have long been considered important tools to test General Relativity in strong-field regimes. In particular, the high frequency quasi-periodic oscillations (HFQPOs) observed in LMXBs binaries containing a black hole candidate have been proposed as a tool for measuring black hole properties such as mass and spin in a direct way. In such systems, the X-ray observations show a particularly rich phenomenology in which the luminosity is modulated quasi-periodically, giving rise to distinctive peaks in the power spectral density. A puzzling feature of the QPO frequencies in these systems is that they are found in sequences of small integers (*i.e.* 1:2, 2:3, or 1:2:3; Abramowicz and Kluźniak, 2001; Remillard et al., 2002; Homan et al., 2003).

Numerous models have been suggested to explain the HFQPOs and their peculiar harmonic property (see Abramowicz and Kluźniak, 2004 for a recent review) but the scarcity of the observational data, on the one hand, and the crudeness of the different models, on the other hand, have not yet made it possible to determine which model provides the most likely description of the pro-

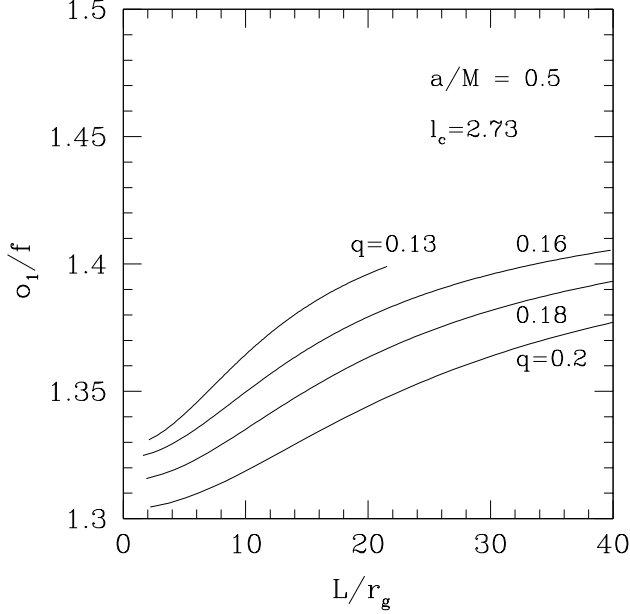


**Figure 8.** Ratio of the first overtone to the fundamental mode shown as a function of the radial extent of the torus  $L$ . The tori are modelled with a power-law distribution of specific angular momentum and the different lines refer to different choices of the index  $q$ , but all assume the same value of  $l_c = 2.73$ .

cesses responsible for the QPOs. It should be noted the first steps towards a more quantitative and physically realistic description of the emission properties of possible QPO models have recently been taken (Schittman and Bertschinger, 2004; Schnittman, 2004).

Among the proposed models, one is particularly simple as it is based on the assumption that the accretion disc around the black hole terminates with a sub-Keplerian part, *i.e.* a torus of small size (Rezzolla et al., 2003a). This model was motivated by the numerical simulations of relativistic tori in a Schwarzschild spacetime (Zanotti et al., 2003) and by the subsequent perturbative study of  $p$ -mode oscillations of relativistic vertically integrated tori presented in Paper I. A Cornerstone of this model is the evidence, both numerical and analytic, that in these objects the fundamental mode and the first overtones are found to be in the harmonic sequence 2:3:4... to a good precision and in a very wide parameter space.

Because the  $p$  modes considered in the above model represent the basic oscillation modes of a non-Keplerian disc, some of their features are not expected to be very sensitive to the properties of the spacetime which determine the motion of the fluid. The harmonic 2:3 relation between the fundamental frequency and the first overtone is one such feature and, indeed, this property has been encountered essentially unmodified in Schwarzschild and Kerr spacetimes, but also in a Newtonian gravitational potential. Because of this, it is then natural to consider whether a fully Newtonian description of the physics is sufficient to account for the phenomenology observed in HFQPOs, or whether General Relativity is indeed necessary. This question is addressed in the following Section.

### 5.1 Can Newtonian Physics explain the HFQPOs?

In order to assess whether  $p$ -mode oscillations in purely Newtonian tori could account for the HFQPO phenomenology, we have performed a global analysis of the axisymmetric oscillations of ver-

tically integrated non-Keplerian discs in Newtonian physics and compared the results with those obtained in a general relativistic framework.

Consider therefore a non-selfgravitating perfect fluid torus in equilibrium and orbiting a central object of mass  $M_0$  producing a gravitational potential  $\Psi$ . As in the general relativistic case, the system of equations describing the torus will be simplified by considering vertically integrated or vertically averaged quantities, which we indicate as  $P$  and  $\Sigma$ , in analogy with the corresponding relativistic quantities (*cf.* eqs. 4 and 5). In order to handle simpler expressions we normalize all quantities as

$$\tilde{v}^i \equiv \frac{v^i}{c_0}, \quad \tilde{\Sigma} \equiv \frac{\Sigma}{\Sigma_0}, \quad \tilde{P} \equiv \frac{P}{P_0}, \quad \tilde{\omega} \equiv \frac{\omega}{\omega_0}, \quad (25)$$

where  $i = \varpi, \phi$ , while  $\Sigma_0$  is the maximum mass density and where we have defined

$$P_0 \equiv K \Sigma_0^{1+1/N}, \quad c_0^2 \equiv \left(1 + \frac{1}{N}\right) \frac{P_0}{\Sigma_0}, \quad \omega_0 \equiv \frac{GM_0}{c_0^2}. \quad (26)$$

The equilibrium configurations are then obtained by solving the hydrostatic equilibrium equation which, in terms of the normalized quantities, is written simply as

$$\frac{1}{\tilde{\Sigma}} \tilde{P}' = \tilde{\Omega}^2 \tilde{\omega} - \tilde{\Psi}', \quad (27)$$

where  $\tilde{\Psi} \equiv \Psi/c_0^2$  and  $\tilde{\Omega} \equiv \Omega/\Omega_0$ , with  $\Omega_0$  being the angular velocity at  $\varpi_0$ . Introducing now the Emden function  $\tilde{\Theta}$  and its related quantity  $\tilde{Q} \equiv N\tilde{\Theta}$ , the normalized rest-mass density  $\tilde{\Sigma}$  can be written as  $\tilde{\Sigma} = \tilde{\Theta}^N$ , and the equation of hydrostatic equilibrium is expressed as an ordinary differential equation for  $\tilde{Q}$ , *i.e.*

$$\tilde{Q}' = \tilde{\Omega}^2 \tilde{\omega} - \frac{1}{\tilde{\omega}^2}. \quad (28)$$

Once the angular velocity distribution  $\Omega = \Omega(\varpi)$  is fixed and a choice is made for the inner radius  $\tilde{\omega}_{\text{in}}$ , equation (28) can be integrated to provide the background Newtonian torus in equilibrium.

For simplicity we now restrict our attention to constant specific angular momentum distributions so that the equation of hydrostatic equilibrium (28) simplifies to

$$\tilde{Q}' = \frac{\ell^2}{\tilde{\omega}^3} - \frac{1}{\tilde{\omega}^2} = - \left( \frac{\ell^2}{2\tilde{\omega}^2} - \frac{1}{\tilde{\omega}} \right)'. \quad (29)$$

Before discussing the solution of the eigenvalue problem, it is useful to recall the features of the Newtonian models that represent important differences from the relativistic counterparts. The first one is that the right-hand side of equation (29) is just the derivative of an effective potential (*i.e.* the one in the round brackets) and it is therefore straightforward to calculate the inner edge of the largest possible torus as the radial position at which this potential vanishes, *i.e.*  $(\tilde{\omega}_{\text{in}})_{\text{MIN}} = \ell^2/2$ .

The second feature to notice is again easily derived from equation (29) and shows that the position of the mass density maximum (*i.e.*  $Q' = 0$ ) is simply given by  $\tilde{\omega}_{\text{max}} = \ell^2$ , coinciding with the position at which the specific angular momentum assumes a Keplerian value. As in relativistic tori,  $\tilde{\omega}_{\text{max}}$  grows with increasing specific angular momentum; unlike relativistic tori, however, no lower or upper limits exist for  $\tilde{\omega}_{\text{max}}$ . Indeed, for vanishingly small values of  $\ell$ , it is possible to construct tori whose pressure maxima lie arbitrarily close to the rotation axis. This property is the consequence of the fact that, in Newtonian physics and for constant distributions of specific angular momentum,  $\ell$  is not constrained to lie in a finite

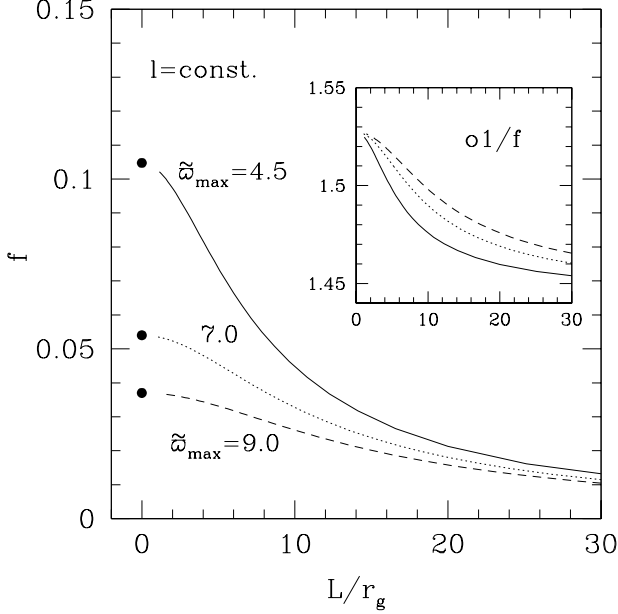


**Figure 9.** Eigenfrequencies of the fundamental mode of oscillation for Newtonian tori with constant angular momentum distribution orbiting a central mass  $M = 10 M_{\odot}$ . We show with solid circles the values of the Newtonian Keplerian radial epicyclic frequency at the different locations of  $\varpi_{\max}$ , while the inset shows the ratio of the first overtone and of fundamental eigenfrequency as a function of the radial extents  $L$ .

interval. This represents a major difference with respect to the general relativistic picture and, as will be discussed later on, makes the parameter space for the background models effectively unbounded.

We next proceed to consider the eigenvalue problem and, as we did for the general relativistic case, we neglect perturbations in the gravitational potential (Cowling approximation) and introduce perturbations in the velocity and pressure with a harmonic time dependence of the type  $\sim \exp(-i\sigma t)$ . To simplify the notation, hereafter we will omit the “tilde” on all variables, which however should be meant to refer to normalized quantities. As a result, the perturbed Euler and continuity equations can be written as

$$\sigma \delta \Sigma + \frac{1}{\varpi} (\varpi \Sigma \delta U)' = 0, \quad (30)$$

$$\sigma \delta U + 2\varpi \Omega \delta W - \delta Q' = 0, \quad (31)$$

$$\left( \Omega' + \frac{2}{\varpi} \Omega \right) \delta U + \sigma \delta W = 0, \quad (32)$$

where, in analogy with the corresponding relativistic quantities,  $\delta U$  and  $\delta W$  are the vertically averaged radial and azimuthal velocities, respectively (*cf.* eqs. 10 and 11).

After some simple algebra, equations (30)–(32) are cast into a single, second-order ordinary differential equation

$$\delta Q'' + \left[ \frac{1}{\varpi} + \frac{Q'}{Q} N + \ln \left( \frac{\sigma}{D} \right)' \right] \delta Q' + \frac{ND}{Q} \delta Q = 0, \quad (33)$$

for the quantity  $\delta Q$  defined as

$$\delta Q \equiv \left( \frac{N}{N+1} \right) \frac{\delta P}{\Sigma}. \quad (34)$$

In equation (33), the quantity

$$D \equiv \sigma^2 - 2\Omega(2\Omega + \varpi \Omega'), \quad (35)$$

measures the deviation of the eigenfrequency  $\sigma$  from the Newtonian radial epicyclic frequency  $(\kappa_r^2)_{\text{Newt}} \equiv 2\Omega(2\Omega + \varpi \Omega')$ , which coincides with the orbital frequency when the orbital motion is Keplerian, *i.e.*  $(\kappa_r)_{\text{Newt}} = \Omega_{\text{Kep}}$ . Note that while equation (33) appears to be singular at the radial position where  $D = 0$ , it is actually regular everywhere since  $\delta Q'$  and  $D$  vanish at the same position (*cf.* eqs. 31 and 32).

The eigenfrequencies and eigenfunctions of the axisymmetric  $p$  modes described by equations (30)–(32) have been computed using the same numerical method discussed in the previous Sections and some representative results are presented in Fig. 9. More specifically, we show the eigenfrequencies of the fundamental mode of oscillation for three sequences of constant angular momentum Newtonian tori orbiting a central source of gravitational potential with a mass of  $10 M_{\odot}$ . The sequences have been built keeping the position of the density maximum fixed (*i.e.*  $\tilde{\varpi}_{\max} = 4.5, 7.0$  and  $9.0$ , respectively) and varying the position of the inner radius to produce tori of different radial sizes. The inset, on the other hand, shows the ratio of the first overtone to the fundamental eigenfrequency as a function of the radial size of the torus for the three different sequences. A first glance at Fig. 9 and a comparison with Figs. 4, 5 and 6, shows that no major *qualitative* differences emerge in a Newtonian framework and that all of the most important features of  $p$  modes in relativistic tori remain unchanged also in the corresponding Newtonian models. Most notably, the fundamental eigenfrequencies depend on the position of the mass density and on the radial sizes of the discs, increasing as the latter decrease. In addition, as the radial sizes tend to zero, the fundamental eigenfrequencies tend to the values of the radial epicyclic frequencies at the position of the mass density maxima. Finally, along all sequences, the first and second eigenfrequencies are in a harmonic sequence 2:3 of small integers.

Besides this qualitative agreement, however, *quantitative* differences are also present and can be easily appreciated by comparing, for instance, the curve for  $a/M = 0$  in the left panel of Fig. 5 with the dotted line in Fig. 9. Indeed, the simultaneous presence of qualitative similarities and quantitative differences between Newtonian and general relativistic models is not surprising and reflects the fact that the  $p$  modes are fundamental modes of oscillation of orbiting fluid objects. As such, they depend only in part on the gravitational field (or background spacetime) in which the fluid is moving. Indeed, also for rotating stars, the qualitative features of the  $p$ -mode oscillations are preserved when going from a Newtonian description to a full general relativistic one, with quantitative differences being present, however, and depending on the strength of the spacetime curvature.

Finally, note that because the radial epicyclic frequencies represent the asymptotic limit of the fundamental eigenfrequencies for vanishing torus sizes and since the Newtonian epicyclic frequency is always *larger* than the corresponding general relativistic one for all values of the black hole spin (*cf.* solid and dotted lines in Fig. 1), all of the Newtonian frequencies along a sequence with  $\ell = \text{const.}$  will be larger than the corresponding relativistic ones. This, together with the fact that the Newtonian epicyclic frequency diverges for vanishingly small radii [*i.e.*  $(\kappa_r)_{\text{Newt}} = \Omega_{\text{Kep}} \sim \tilde{\varpi}^{-3/2}$ ], makes it clear that for any observed QPO frequency it will be possible to find a Newtonian torus of size  $L$  that could produce  $p$  mode oscillations with the correct frequencies and in a 2:3 ratio. Stated differently, while the parameter space

in the  $(f, L)$  plane for relativistic tori is bounded above by the sequence approaching the largest epicyclic frequency admissible by a Kerr black hole with spin  $a/M = 1$ , this restriction does not exist for Newtonian tori and a Newtonian physicist, who ignores the existence of marginally stable orbits or of an event horizon, would be able to find an equilibrium solution at every point in that plane.

As a result, and at least in principle, Newtonian physics could explain the HFQPOs if the only information available is the mass of the central object  $M$  and the frequencies of the modulation in the X-ray luminosity  $\sigma$ . The only way to remove this ambiguity and thus disprove the interpretation of the Newtonian physicist, would be to make combined measurements of  $M$  and  $\sigma$ , together with the radial extension of the torus  $L$ , or of the position of the mass density maximum  $\varpi_{\max}$ . While both these observations would probably be difficult to make in practice, similar difficulties are found also in proving the existence of stellar-mass black holes in X-ray binaries (Abramowicz, Kluźniak and Lasota, 2002). This is simply the consequence of the fact that no limit exists in Newtonian physics to the compactness of the sources of gravitational potential.

## 6 CONCLUSIONS

We have presented the study of the oscillation properties of non-selfgravitating tori orbiting around Kerr black holes. This work extends the previous investigations of the oscillation properties of relativistic tori in a Schwarzschild background and their importance in explaining the HFQPOs in X-ray binaries containing a black hole candidate (Rezzolla et al., 2003a). Following the same approach presented in these previous works, we have here considered the axisymmetric  $p$ -mode oscillations of relativistic tori assuming a vertically integrated description to reduce the eigenvalue problem to the solution of a system of coupled ordinary differential equations.

We have first considered a local analysis in a Kerr spacetime and determined the relations between acoustic and inertial waves, showing that both are present in the oscillations of geometrically thick discs and that they play a different role depending on the radial size of the disc and on the position of the rest-mass density maximum. We have then computed the eigenfunctions and the eigenfrequencies of the axisymmetric  $p$  modes for a large variety of background models which differed either in the spin of the black hole or in the distributions of specific angular momentum considered. The latter, in particular, have been considered to be constant or to increase outwards following a power-law in radius.

On the whole, the  $p$ -mode oscillations of vertically integrated tori in a Kerr spacetime possess all of the most important features already encountered in a Schwarzschild spacetime. Firstly, the fundamental eigenfrequencies depend on the position of the rest-mass density maximum and on the radial size of the discs, increasing as the latter decreases. Secondly, the fundamental eigenfrequencies tend to the values of the radial epicyclic frequencies at the position of the mass density maxima as the radial sizes of the tori tend to zero. Finally, for tori constructed with constant distributions of specific angular momentum, the first and second eigenfrequencies are in a harmonic sequence 2:3 of small integers. This ratio is not exact but is very accurately satisfied with deviations of  $\sim 10\%$  at most. For non-constant distributions of angular momentum, on the other hand, the harmonic sequence is still present for sufficiently large tori, but the deviation from a precise 2:3 ratio increases, being  $\sim 20\%$  at most.

We have also investigated the implications that  $p$ -mode oscillations could have on the HFQPOs observed in X-ray binaries

containing a black hole candidate. In a model recently proposed, the presence of a sub-Keplerian flow (*i.e.* a torus) near the black hole and its oscillations are used to explain many of the features of the HFQPOs and, in particular, the 2:3 ratio in the peaks of the power spectral density (Rezzolla et al., 2003a). In this model, the measure of the oscillation frequencies and the knowledge of the  $p$ -mode properties can be used to measure directly the black hole properties, such as the mass and spin, once a reasonable estimate of the torus size is made.

In view of this, we have considered whether an equivalent interpretation of the HFQPOs phenomenology can also be made in terms of a purely Newtonian description of physics. To this scope, we have performed a global analysis of vertically integrated Newtonian tori following the same mathematical and numerical approach developed for tori in a Kerr spacetime. Our results indicate that, at least *qualitatively*, the  $p$ -mode oscillations of Newtonian tori preserve all of the properties encountered in their relativistic counterparts. Furthermore, while *quantitative* differences do exist between the two frameworks, it may be difficult to distinguish between the two unless the oscillation frequencies are measured together with the radial extension of the torus  $L$ , or through the measurement of the position of the mass density maximum  $\varpi_{\max}$ .

## ACKNOWLEDGMENTS

It is a pleasure to thank Marek Abramowicz, Omar Blaes, Toni Font, and Wlodek Kluźniak for many useful discussions. We are also grateful to John Miller and Tom Maccarone for carefully reading the manuscript and to Olindo Zanotti for a close comparison of our results with his numerical simulations. Financial support has been provided by the MIUR and INFN (OG51). SY is supported by the NSF grant PHY 0071044 and acknowledges support from the INFN while visiting SISSA. The computations were performed on the Beowulf Cluster for numerical relativity “*Albert100*”, at the University of Parma.

## REFERENCES

- Abramowicz, M.A., Calvani, M., Nobili, L., 1983, *Nature*, 302, 597
- Abramowicz, M.A., Prasanna, A.R., 1985, *MNRAS*, 245, 720
- Abramowicz, M.A., Kluźniak, W., 2001, *A&A*, 374, L19
- Abramowicz, M.A., Kluźniak, W., Lasota, J.-P., 2002, *A&A*, 396, L31
- Abramowicz, M.A., Kluźniak, W., 2004, *Proceedings of “X-ray Timing 2003: Rossi and Beyond”*, ed. P. Kaaret, F.K. Lamb, and J.H. Swank
- Aschenbach, B., Grosso, N., Porquet, D., Predehl, P., 2004, *A&A*, 417, 71
- Blaes, O.M. 1985, *MNRAS*, 216, 553
- Cowling, T.G., 1941, *MNRAS*, 101, 367
- Daigne, F., Font, J.A., 2004, *MNRAS*, 349, 841
- De Villiers, J.-P., Hawley, J. F., Krolik, J. H., 2003 *ApJ*, 599 1238
- Font, J.A., Daigne, F., 2002a, *MNRAS*, 334, 383
- Font, J.A., Daigne, F., 2002b, *ApJ*, 581, L23
- Homan, J., Miller, J.M., Wijnands, R., Steeghs, D., Belloni, T., van der Klis, M., Lewin, W.H.G., 2003, *ATel* 162
- Giannios, D., Spruit, H.C., 2004, *A&A*, in press
- Kato, S., 2001, *PASJ*, 53, 1
- Kluźniak, W., Abramowicz, M.A., Kato, S., Lee, W.H., Stergioulas, N., 2004, *ApJ*, 603, L89
- Kozłowski, M., Jaroszynski, M., Abramowicz, M.A., 1978, *A&A*, 63, 209
- Lee, W.H., Abramowicz, M.A., Kluźniak, W., 2004, *ApJ*, 603, L93
- Novikov, I., Thorne, K.S., 1973, in *Black Holes*, eds. B. de Witt and C. de Witt, Gordon and Breach, NY 491, 663
- Okazaki, A. T., Kato, S., Fukue, J., 1987, *PASJ*, 39, 457

- Perez, C.A., Silbergleit, A.S., Wagoner, R.V., Lehr, D.E., 1997, *ApJ*, 476, 589
- Press, W.H., Flannery, B.P., Teukolsky, S.A., and Vetterling, W.T., *Numerical Recipes*, Cambridge University Press, Cambridge (1986).
- Remillard, R. A., Morgan, E. H., McClintock, J. E., Bailyn, C. D., Orosz, J. A., 1999, *ApJ*, 522, 397
- Remillard, R.A., Muno, M.P., McClintock, J.E., Orosz, J.A., 2002, *Astrophys. J.*, 580, 1030
- Rezzolla, L., Yoshida, S'i., Maccarone, T. J., Zanotti, O., 2003a, 344, L37
- Rezzolla, L., Yoshida, S'i., Zanotti, O., 2003b, *MNRAS* 344, 978
- Rodriguez, M.O., Silbergleit, A.S., Wagoner, R.V., 2002, *ApJ*, 567, 1043
- Schnittman, J. D., Bertschinger, E., 2004, *ApJ*, 606, 1098
- Schnittman, J. D., 2004, [astro-ph/0407179](#)
- Seguin, F.H., 1975, *ApJ*, 197, 745
- Silbergleit, A.S., Wagoner, R.V., Rodriguez, M., 2001, *ApJ*, 548, 335
- Strohmer, T.E., 2001, *ApJ*, 552, L49
- Tassoul, J.L., 1978, in *Theory of Rotating Stars*, Princeton University Press
- Zanotti, O., Rezzolla, L., Font, J.A., 2003, *MNRAS*, 341, 832
- Zanotti, O., Font, J.A., Montero, P.J., Rezzolla, L., 2004, in preparation

first and the second one, for which the radial derivative introduces a factor  $ik$  balancing the smallness of  $\tilde{\Gamma}$ .

## APPENDIX A: ON THE DISPERSION RELATION FOR TORI AROUND KERR BLACK HOLES

We here briefly discuss the simplifications of equations (12)–(14) that lead to the homogeneous linear system with matrix form (15). In particular, we start from the analogy of equation (12) with its Newtonian counterpart, equation (31), whose pressure-gradient term  $\delta Q'$  and centrifugal term  $2\varpi\Omega\delta W$  are of about the same order. The reason for this is that the inertial-acoustic modes are the results of small deviations from the equilibrium between the centrifugal force and the pressure gradients, which produce the small perturbative radial velocity field expressed by the first term in equation (31).

We expect this to be true also in the general relativistic case and assume, therefore, that the second and the third terms in equation (12) are of the same order. We also note that since  $u^t = \mathcal{O}(1)$ , then  $\alpha = \mathcal{O}(1)$  and thus the leading order coefficient in the square bracket multiplying  $\delta W$  is the first one, *i.e.*  $(\Delta^{3/2}/A)(A/\varpi^2)'\Omega$ .

Because now  $\Delta \sim \varpi^2$  and  $A \sim \varpi^4$ , it is not difficult to show that the ratio of the third to the first term in equation (12) is given by

$$\frac{\alpha(\Delta/\varpi^2)\delta Q'}{(\Delta^{3/2}/A)(A/\varpi^2)'\Omega\delta W} \sim \frac{k}{\Omega} \frac{\delta Q}{\delta W}, \quad (\text{A1})$$

where we have replaced radial derivative with a factor  $ik$ . Since we assume the ratio (A1) to be  $\mathcal{O}(1)$ , we can deduce that

$$\frac{\delta W}{\delta Q} \sim \frac{k}{\Omega}. \quad (\text{A2})$$

Using now this order of magnitude estimate, we can consider the azimuthal Euler equation (13) and evaluate the ratio between the first and third terms, which is given by

$$\frac{(\sigma\varpi^2\sqrt{\Delta}/A)\delta W}{[A\sigma\alpha(\omega - \Omega)/\Delta\varpi^2]\delta Q} \sim \frac{1}{\Omega} \frac{\delta W}{\delta Q} \sim \frac{k}{\Omega^2}, \quad (\text{A3})$$

As a result, in the limit of large wavenumbers considered here (*i.e.* for  $k \rightarrow \infty$ ), the third term in equation (13) can be neglected when compared with the first one.

Finally, in the continuity equation (14), we note that all of the terms except the first one are multiplied by  $\tilde{\Gamma}$  or comparable terms [*e.g.*  $P'/(E + P)$ ]. The latter is rather small and of the order  $\sim (c_s/c)^2$ , where  $c_s$  and  $c$  are local sound speed and the speed of light, respectively. As a result, the leading terms we retain are the